Density dependence of the stopping mean excitation energy

James M. Peek
Los Alamos National Laboratory, Los Alamos, New Mexico 87545
(Received 20 July 1987)

The local-plasma model for the stopping mean excitation energy $I(0)$ of Lindhard and Scharff is used to investigate the effects of target density. The use of the Thomas-Fermi electron density produces a universal curve for $I(0)/Z$, where Z is the nuclear charge number, as a function of the target density. Experimental data for $I(0)$ are shown to be in good agreement with this predicted curve. A simple formula is derived for $I(0)$ in the limit of high target density. This approach is known to predict a similar curve for the charge dependence of $I(0)/Z$ for atomic ion targets. Numerical comparisons and an asymptotic formula for the large-charge limit are presented for this case.

The local-plasma model of Lindhard and Scharff[1] defines the stopping mean excitation energy $I(0)$ in terms of the target radial electron density $\rho(r)$ as

$$\ln[I(0)/H]=[2N(r_0)]^{-1}\int_0^{r_0} dr\, 4\pi r^2\rho(r) \times\ln[\gamma^2 4\pi\rho(r)a_0^3]\ , \tag{1}$$

where

$$N(r_0)=\int_0^{r_0} dr\, 4\pi r^2\rho(r)\ . \tag{2}$$

H is the Hartree unit of energy, a_0 is the Bohr unit of length, and γ is an empirical constant. The usual infinite range for r and normalization condition have been replaced by conditions that anticipate the following developments. Equation (1) has proved very useful in correlating experimental data. For example, Chu and Powers[2] obtained excellent agreement with experiment by using the Herman-Skillman[3] free-atom orbitals and $r_0\to\infty$ to determine $\rho(r)$. The choice of $\gamma\neq 1$ has caused some discussion, and it was noted[4] that the use of $\rho(r)$ from a cell model for solid targets, which implies a finite r_0, increases the predicted $I(0)$ over the free-atom prediction. This allowed a choice for γ nearer to unity than the original suggested value[1] of $\sqrt{2}$ but did not remove its presence. Many detailed discussions of the nature of this theory and the choices for γ are available.[5]

Equation (1) is used here with the Thomas-Fermi[6] formula for $\rho(r)$ and a cell model for the target to amplify the observations made in Ref. 4. This approach results in a curve for $I(0)/Z$, where Z is the nuclear charge number that applies to all neutral targets and depends only on the density of the target. This is very similar to and is a generalization of the result found by Bloch[7] that predicted $I(0)/Z$ to be a constant for all targets.

The Thomas-Fermi equation for the electron radial density is

$$4\pi\rho(r)=(Z^2/b^3)[\varphi(x)/x]^{3/2}\ , \tag{3}$$

where

$$b=(9\pi^2/128)^{1/3}a_0\ ,$$

$$x=Z^{1/3}r/b\ ,$$

and

$$\frac{d^2\varphi(x)}{dx^2}=\frac{[\varphi(x)]^{3/2}}{x^{1/2}} \tag{4}$$

determines $\varphi(x)$ subject to the conditions $\varphi(0)=1$ and the derivative of $\varphi(x)$ at $x=0$, $\varphi'(0)=-S$, be specified. Substituting Eq. (3) into Eqs. (1) and (2) gives

$$I(0)/(ZH)=\gamma\exp\left\{[2f(x_0)]^{-1}\int_0^{x_0} dx\,\sqrt{x}\,[\varphi(x)]^{3/2}\ln\{(b/a_0)^{-3}[\varphi(x)/x]^{3/2}\}\right\}\ , \tag{5}$$

with[6]

$$f(x_0)\equiv N(x_0)/Z=\int_0^{x_0} dx\,\sqrt{x}\,[\varphi(x)]^{3/2}\ . \tag{6}$$

The function $\varphi(x)$ for $S<1.588\,07$ (Ref. 8) implies the density for a neutral atom confined to a sphere of radius r_0 (Ref. 6) or, equivalently, x_0. $Z=N(x_0)$, or $f(x_0)=1.0$, defines the radius of the neutral sphere.

Equations (5) and (6) show that $I(0)/Z$ is a universal function of x_0 for the Thomas-Fermi approximation to $\rho(r)$. A value for x_0 is obtained from the target's density by requiring the volume of a sphere of radius x_0 be equal to the apparent volume that is occupied by an atom in the target being considered.[9]

The resulting universal curve for single-component neutral materials is shown in Figs. 1 and 2. The high-density or small-x_0 limit

$$I(0)/(ZH)\simeq\gamma e^{1/4}\{2[(b/a_0)x_0]^{-3}\}^{1/2} \tag{7}$$

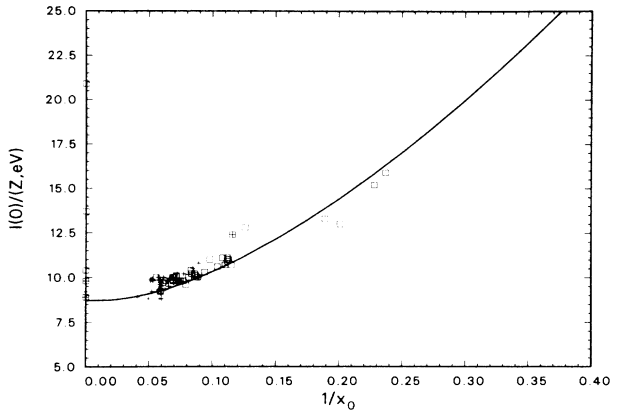

FIG. 1. Value of $I(0)/Z$ as defined by Eq. (5) is shown by the solid line as a function of x_0^{-1}. Experimental values from Ref. 10 for the elements are shown by the squares and interpolated values by $+$.

is derived in the Appendix and is shown in Fig. 2.

Experimental data[10] for the elements are also shown in Fig. 1. It seems clear that the trend with density or, equivalently, x_0^{-1} predicted by Eq. (5) is in agreement with experiment. The largest differences occur for gaseous targets, $x_0^{-1} \simeq 0$. These calculations used $\gamma = 1.41$, in accord with the value that reasonably reproduces experimental values,[1,2] where it should be noted that comparisons of Eq. (1) with other theoretical data indicate a smaller value.[4,5,11]

The cell model is relatively successful in describing the bonding nature of solids[9] under a variety of conditions. Hence, the curve in Figs. 1 and 2 gives a prediction for the behavior of this stopping parameter under extreme conditions such as those encountered in astrophysical environments or, potentially, in laboratory inertially confined fusion experiments.[12]

This model does not make a distinction between phase and chemical-bonding effects. However, it is clear that $I(0)/Z$ is predicted to be less for tenuous materials than it is for solids. This is consistent with the qualitative observation that stopping for a gas or vapor tends to exceed that for the corresponding solid.[13] The cell model as used here is not well suited for application to molecular targets but estimates can be constructed. For example, consider water as a sphere with the density-radius dependence defined above. This is not accurate for predicting absolute values since a Z value is not clearly defined. However, if $Z = 10$ and the normal densities[10] are used to estimate values for x_0, the liquid-vapor and ice-vapor ratios for $I(0)$ are predicted, from the curve in Fig. 1, to be 1.20 and 1.19. The ice-vapor ratio is not known experimentally but a theoretical calculation[14] predicts 1.20. The liquid-vapor ratio is recommended to be 1.13 (Ref. 13) while other values, 1.05, are in use.[10,14] Typically, this method will overestimate the condensed-tenuous ratios because the values for tenuous targets tend to be too small (see Fig. 1). Examples for composite materials will not be considered and, unfortunately, there are no data for compressed targets.

The case of ions with positive charge corresponds to solutions of Eq. (4) with $S > 1.588\,08$.[8] In this case, $\varphi(x_0) = 0$ defines x_0 and, through Eq. (6), $f(x_0) < 1.0$.[6] Equation (5) again shows that, with these approximations, $I(0)/Z$ is a function of a single variable, either x_0 or $f(x_0)$. It is more natural to use $f(x_0)$ as the independent variable for ionized atomic targets. The results for Eq. (5) are shown in Fig. 3 along with the small $f(x_0)$ or large ion-charge limit,

$$I(0)/(ZH) \simeq \gamma e^{1/2}\{\pi[16(b/a_0)^3 f(x_0)]^{-1}\}^{1/2} , \quad (8)$$

which is derived in the Appendix.

The prediction of a universal curve by Eq. (5) for positive ions is known and Ref. 12 provides a convenient and accurate expression for Eq. (5) in this case. There are no experimental data for ionic targets but, since such data are required in the modeling of high-temperature plasmas, some theoretical data are available. The data

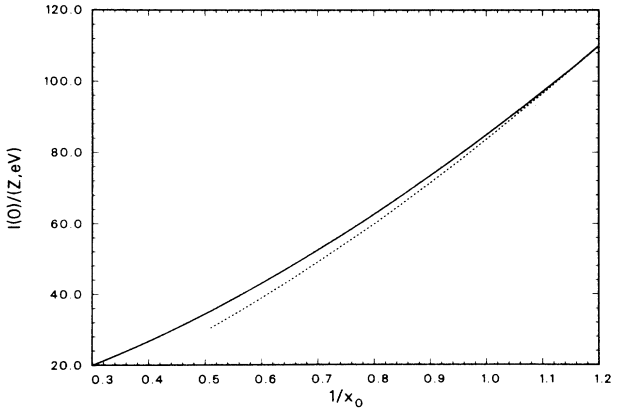

FIG. 2. Behavior of $I(0)/Z$ vs x_0^{-1}, as defined by Eq. (5) is shown as the solid line and the dashed line represents the high-density limiting behavior given by Eq. (7).

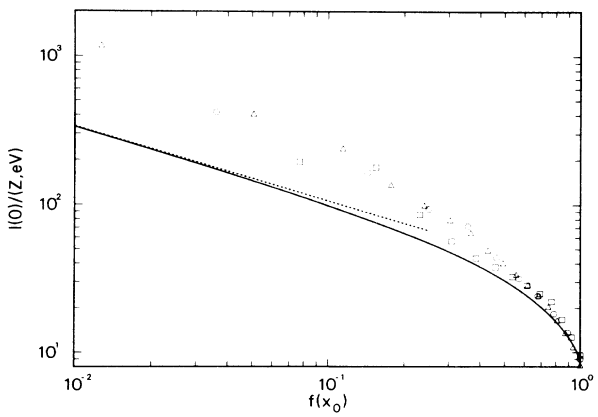

FIG. 3. Prediction of Eq. (5) for ions is shown as a function of $f(x_0)$ by the solid line. The dashed line represents the high-ionization limiting behavior given by Eq. (8). Theoretical data calculated by the techniques of Ref. 15 are shown by squares for Al, by circles for Ni, and by triangles for Au.

shown in Fig. 3 are either presented in Refs. 15 and 16 or are from unpublished calculations.[15] The agreement between the two types of calculations is reasonably good for $f(x_0)>0.5$, noting that the logarithmic scales used in Fig. 3 tend to diminish differences. Also, the average error could be reduced by an increase in the value of γ.

The marked increase in error for Eq. (5) and $f(x_0)\approx 1/Z$ is anticipated because of the failure of Eq. (1) to scale correctly in this limit.[11] The correct $I(0)\propto Z^2$ scaling as $f(x_0)$ approaches $1/Z$ is replaced by $I(0)\propto Z^{3/2}$ when quantum orbitals are used to evaluate Eq. (1). The Thomas-Fermi approximation to $\rho(r)$ can be seen from Eqs. (6) and (8) to reproduce the same error.

The important point displayed in Fig. 3 is the tendency of available data to follow a universal curve in these variables even if it is not the one predicted by Eq. (5). In fact, a crude adaptation of Eq. (8) suggested by Fig. 3,

$$I(0)/(Z\ \text{eV})=(33/f^{0.85})-23\ ,$$

is a reasonable fit for all $f(x)$.

APPENDIX

The derivation of the high-density limit, Eq. (7), is presented first. For $0\le x\le x_0$ the assumption

$$\varphi(x)\simeq 1-Sx+cx^2$$

is used. Equation (6) requires

$$1=\int_0^{x_0} dx\,\sqrt{x}\,[\varphi(x)]^{3/2}=\int_0^{x_0} dx\,x\left[\frac{d^2\varphi(x)}{dx^2}\right]\simeq cx_0^2\ .$$

The direct evaluation of Eq. (5), using the following order of approximation,

$$\begin{aligned} I(0)/(ZH)&=\gamma\exp\left[(\tfrac{1}{2})\int_0^{x_0} dx\,x\,[d^2\varphi(x)/dx^2]\ln\{[x^{-1}(b/a_0)^{-3}][d^2\varphi(x)/dx^2]\}\right]\\ &\simeq\gamma\exp\left[(\tfrac{1}{2})\int_0^{x_0} dx\,(2x/x_0^2)\ln\{2x^{-1}x_0^{-2}(b/a_0)^{-3}]\}\right]\ , \end{aligned}$$

to give Eq. (7), is an easy calculation.

The highly ionized limit to Eq. (5) is obtained by assuming

$$\varphi(x)\simeq 1-Sx$$

and, since

$$\varphi(x_0)=0$$

determines x_0 for this case,

$$S\simeq x_0^{-1}$$

is required. Substituting this into Eqs. (6) and (5) produces

$$f(x_0)\equiv N(x_0)/Z\simeq(\pi/16)x_0^{3/2}$$

and

$$\begin{aligned} &\int_0^{x_0} dx\,\sqrt{x}\,[\varphi(x)]^{3/2}\ln\{(b/a_0)^{-3}[\varphi(x)/x]^{3/2}\}\\ &\quad\simeq\int_0^{x_0} dx\,\sqrt{x}\left[1-\left[\frac{x}{x_0}\right]\right]^{3/2}\\ &\qquad\times\ln\left[\left[\frac{b}{a_0}\right]^{-3}\left[\frac{1-x/x_0}{x}\right]^{3/2}\right]\\ &\quad=(\pi/16)x_0^{3/2}\{1-\ln[(b/a_0)^3x_0^{3/2}]\}\ , \end{aligned}$$

which, when substituted into Eq. (5), gives Eq. (8).

[1] J. Lindhard and A. Scharff, K. Dan. Vidensk. Selsk. Mat.-Fys. Medd. **27**(15) (1983).

[2] W. K. Chu and D. Powers, Phys. Lett. **40A**, 23 (1972).

[3] F. Herman and S. Skillman, *Atomic Structure Calculations* (Prentice-Hall, Englewood Cliffs, NJ, 1963).

[4] J. F. Ziegler, *Stopping and Ranges of Ions in Matter* (Pergamon, New York, 1980), Vol. 5.

[5] R. E. Johnson and M. Inokuti, Comments At. Mol. Phys. **14**, 19 (1983).

[6] H. A. Bethe and R. Jackiw, *Intermediate Quantum Mechanics* (Benjamin, New York, 1968), Chap. 5.

[7] F. Bloch, Z. Phys. **81**, 363 (1933); E. Bonderup, K. Dan. Vidensk. Selsk. Mat.-Fys. Medd. **35**(17) (1967).

[8] See, for example, S. Kobayashi, T. Matsukuma, S. Nagi, and K. Umeda, J. Phys. Soc. Jpn. **10**, 759 (1955).

[9] G. K. Straub and W. A. Harrison, Phys. Rev. B **31**, 7668 (1985).

[10] M. J. Berger and S. M. Seltzer, National Bureau of Standards Report No. NBSIR 82-2550, 1982 (unpublished).

[11] J. M. Peek, Phys. Rev. A **26**, 1030 (1982).

[12] R. M. More, in *Proceedings of the Scottish Universities Summer School in Physics,* St. Andrews, 1985, edited by M. B. Hooper (Scottish Universities Summer School in Physics, Edinburgh, 1986), pp. 157–214.

[13] D. I. Thwaites, Nucl. Instrum. Methods Phys. Res. B **12**, 84 (1985); L. E. Porter and D. I. Thwaites, Phys. Rev. A **25**, 3407 (1982).

[14] J. A. LaVerne and A. Mozumder, J. Phys. Chem. **90**, 3242 (1986).

[15] J. M. Peek, L. C. Pitchford, and E. J. Shipsey, Phys. Rev. A **29**, 1096 (1984).

[16] E. J. McGuire, J. M. Peek, and L. C. Pitchford, Phys. Rev. A **26**, 1318 (1982).